Collisions of Deformed Nuclei and Superheavy-Element Production

Akira Iwamoto†, Peter Möller†‡§¶, J. Rayford Nix¶, and Hiroyuki Sagawa‡

†Advanced Science Research Center, Japan Atomic Energy Research Institute, Tokai, Naka-gun, Ibaraki, 319-11 Japan

‡Center for Mathematical Sciences, University of Aizu, Aizu-Wakamatsu, Fukushima 965-80, Japan

§P. Moller Scientific Computing and Graphics, Inc., P. O. Box 1440, Los Alamos, NM 87544, USA

¶Theoretical Division, Los Alamos National Laboratory, Los Alamos, NM 87545, USA

Abstract. A detailed understanding of complete fusion cross sections in heavy-ion collisions requires a consideration of the effects of the deformation of the projectile and target. Our aim here is to show that deformation and orientation of the colliding nuclei have a very significant effect on the fusion-barrier height and on the compactness of the touching configuration. To facilitate discussions of fusion configurations of deformed nuclei, we develop a classification scheme and introduce a notation convention for these configurations. We discuss particular deformations and orientations that lead to compact touching configurations and to fusion-barrier heights that correspond to fairly low excitation energies of the compound systems. Such configurations should be the most favorable for producing superheavy elements. We analyse a few projectile-target combinations whose deformations allow favorable entrance-channel configurations and whose proton and neutron numbers lead to compound systems in a part of the superheavy region where α half-lives are calculated to be observable, that is, longer than 1 μs.

1. Introduction

The last five elements that have been discovered [1–5] were all formed in cold-fusion reactions between spherical nuclei. As the proton number increases, the cross section for heavy-element production decreases. For example, element 107 was produced with a 167 pb cross

section [1], whereas for element 111 the production cross section was only 2–3 pb [5]. There is reason to suspect that few additional new elements can be reached in reactions between spherical nuclei because of the strong decreasing trend of the cross sections.

In fusion reactions where the number of protons in the projectile and target add up to about 100, the overwhelming inelastic cross-section component is fusion-fission. In a classical picture a necessary condition for complete fusion and the formation of a compound nucleus is that the fusing system evolves into a configuration inside the fission saddle point in a multi-dimensional deformation space [6–9]. In heavy-ion collisions where the projectile and target are of roughly equal size and with a nucleon number A above about 100, the touching configuration is outside the fission saddle point on the side of a steep hill [10]. For energies just above the Coulomb barrier this topographical feature results in a trajectory that is deflected away from the direction towards the spherical shape. Instead, it leads from the touching configuration to the fission valley, so that no compound-nucleus formation occurs.

There are two simple possibilities that immediately suggest themselves to overcome the above limitation to compound-nucleus formation and increase the cross section for heavy-element production. First, if the projectile energy is increased, the trajectory will, for sufficiently high energy, pass inside the fission saddle point. However, frictional forces may make such trajectories difficult to realize. Second, highly asymmetric touching configurations may be sufficiently close to the ground-state shape of the compound nucleus that the touching configuration is inside the fission saddle point. Thus, these two simple principles would suggest that to produce elements in the superheavy region one should select highly asymmetric configurations and increase the projectile energy above the Coulomb barrier. However, high excitation energies and resultant high angular momenta of the compound system may favor fission instead of de-excitation by neutron emission. In the cold-fusion approach that led to the identification of the five heaviest elements the very nature of cold fusion leads to a low excitation energy of the compound system. The entrance-channel configuration is also fairly asymmetric and compact. However, the maximum cross section for the production of the heaviest elements occurs at sub-barrier energies as very rare, non-classical events.

Our discussion above revealed that from very general principles one can expect that heavy-element production in heavy-ion reactions is most favorable when the touching configuration is compact. The excitation energy of the compound system should be high enough to allow a trajectory inside the fission saddle point, but as low as possible to reduce the fission branch of the compound system. A spherical picture of nuclei in heavy-ion collisions allows few new possibilities for very-heavy-element production beyond what has already been accomplished. It is therefore of interest to investigate if consideration of deformation will identify entrance-channel configurations that have some possibility of being more favorable for heavy-element production than is expected from the spherical picture.

To facilitate the discussion of deformed fusion configurations we introduce a classification scheme, notation and terminology.

2. Fusion configurations of deformed nuclei: Classification, notation and terminology

Obviously, the multi-dimensional fusion potential is a continuous function of the incident direction and orientation of the projectile nucleus and of the deformation of the projectile and target. However, to allow the identification and discussion of major physical effects it is useful to identify and study a few limiting situations.

2.1. Limiting fusion configurations

Our discussions of specific cases below will show that for prolate shapes there are significant differences in the fusion process depending on the sign of the hexadecapole moment. Nuclei with a large negative hexadecapole moment develop a neck which allows a close approach. As a result the fusion configuration for some orientations of the projectile-target combinations is considerably more compact than the corresponding configurations for shapes with large positive hexadecapole moments. Thus, we identify four limiting situations as far as deformations are concerned. They are:

1. Well-developed oblate shapes
2. Spherical shape
3. Well-developed prolate shapes with large negative hexadecapole moments Q_4
4. Well-developed prolate shapes with large positive hexadecapole moments Q_4

Furthermore, we assume mass symmetry and axial symmetry as this is consistent with the vast majority of nuclear ground-state configurations.

In our studies here we use alternatively the Nilsson perturbed-spheroid parameterization ϵ [11] and the β parameterization to generate deformed nuclear shapes. In the β parameterization, assuming axial symmetry, the radius vector $R(\theta, \phi)$ to the nuclear surface is defined by

$$R(\theta, \phi) = R_0 \left[1 + \sum_{l=1}^{\infty} \beta_l Y_l^0(\theta, \phi) \right] \tag{1}$$

where R_0 is deformation dependent so as to conserve the volume inside the nuclear surface. The variation in R_0 due to volume conservation is only a fraction of one percent. The definition of the ϵ parameterization is more complicated. A recent, extensive presentation is given in Ref. [12]. One should note that large positive Q_4 corresponds to positive β_4 but to negative ϵ_4 and that large negative Q_4 corresponds to negative β_4 but to positive ϵ_4.

As limiting orientations we consider only situations where the projectile center is on the x, y or z axis of the target and orientations of the projectile where the projectile symmetry axis is either parallel to or perpendicular to the target symmetry axis. Since we restrict ourselves to axial symmetry, configurations with the projectile center located on the x or y axis are identical. If the projectile is located in the equatorial region of the target it can be oriented in three major orientations, and if it is located in the polar region it can be oriented in two major orientations. Thus, for a particular projectile-target deformation combination there are five possible limiting configurations.

Because there are five orientations and three major types of deformations for both projectile and target there are 45 different configurations when the projectile and target are deformed and of unequal mass. When the projectile and target are of equal mass, one would at first sight expect 30 different configurations. We later show that in the case of equal projectile and target mass there are three pairs of configurations where the two configurations in the pairs are identical. Therefore, there are in this case only 27 deformed configurations that are different. Situations where either the projectile or target is deformed add another six configurations and, finally, we designate a spherical target and a spherical projectile as a separate configuration. Thus, in our classification scheme we find 34 configurations of projectile and target in heavy-ion collisions that are different also in the special case of equal projectile and target mass. For the case of unequal projectile and target mass one may wish to count a total of 45 different deformed configurations, for a total of 52 different fusion configurations.

We will in a separate study systematically review the barrier parameters of these configurations for projectiles and targets throughout the periodic system. Here, we will just discuss a few configurations with potential importance for very-heavy-element production. However, to be able to simply and transparently refer to any of the limiting configurations we start by introducing a notation convention for deformed fusion configurations.

2.2. Notation for deformed fusion configurations

We denote a particular fusion configuration by [P,T,O], where the three letters stand for Projectile deformation, Target deformation, and relative Orientation of the projectile-target combination. For configurations where the projectile or target or both are spherical, the number of different limiting orientations is less than when both the projectile and target are deformed. It is therefore most clear to introduce notation that distinguishes between these possibilities. The following values are possible for the three entities P, T and O:

P and T

- Oblate: ..... o
- Spherical ..... s
- Prolate with negative Q_4 ..... p^-
- Prolate with positive Q_4 ..... p^+

O Spherical projectile and spherical target

- Spherical (s) ..... ○◯

O Spherical-deformed projectile-target combination

- Polar (p) ..... °|
- Equatorial (e) ..... ○|

O Deformed-deformed projectile-target configuration

- Polar-transverse (pt) ..... ⊤
- Polar-parallel (pp) ..... ||
- Equatorial-transverse (et) ..... ⊣
- Equatorial-parallel (ep) ..... ||
- Equatorial-cross (ec) ..... ┼

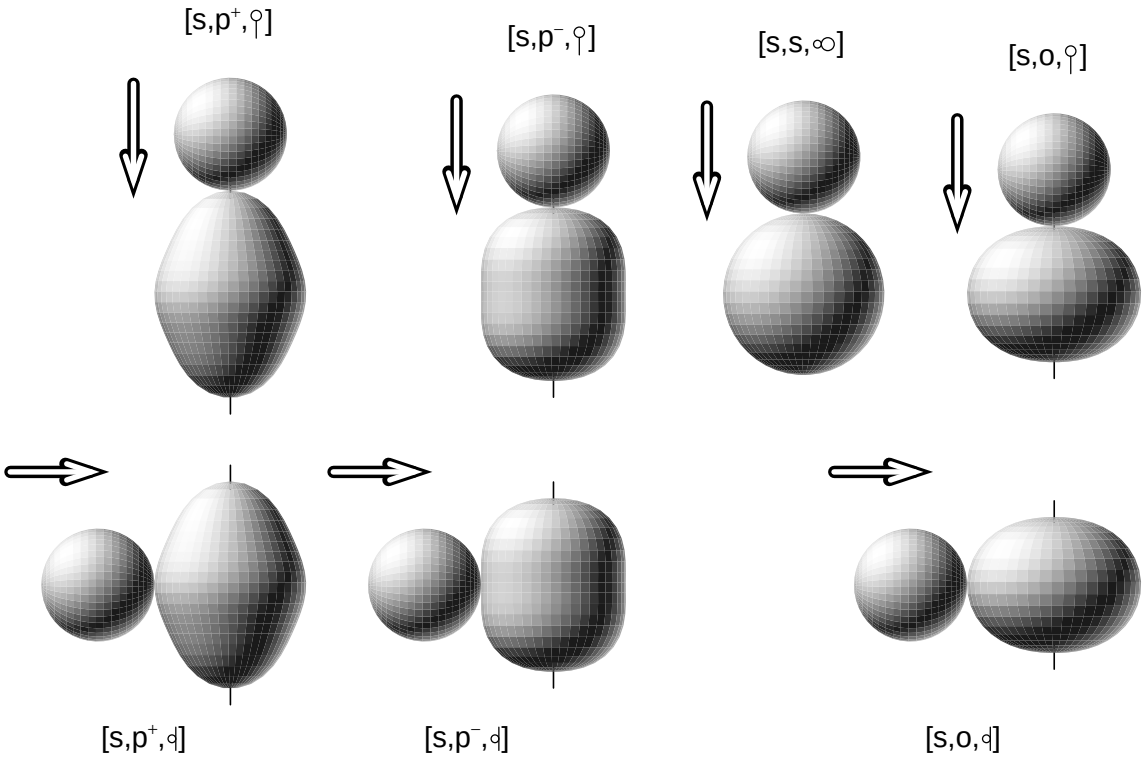

Figure 1. The seven limiting touching configurations with spherical projectiles. The simplest configuration with a spherical target is in the top row third from the left. To the left of this configuration are configurations with prolate target shapes whereas to the right are the two limiting configurations that occur for oblate target shape. The ratio between the projectile and target volume is 0.343. The deformation is $\beta_2 = 0.30$ and $\beta_4 = 0.11$ for p^+, $\beta_2 = 0.24$ and $\beta_4 = -0.09$ for p^-, and $\beta_2 = -0.25$ and $\beta_4 = 0.0$ for o shapes. The arrows give the direction of the incident beam. The nuclear symmetry axis is indicated by a thin line emerging from the nuclear polar regions.

We prefer the graphical short-hand notation given in the table above for the different orientations, but we also provide in parenthesis an alternative notation, based on letters only.

In Fig. 1 we show the seven different configurations that can occur with a spherical projectile. We have sandwiched the familiar spherical-projectile spherical-target case between the prolate-target and oblate-target configurations in the top row so that the appearance of the configurations evolves smoothly from the polar, spherical-prolate positive-hexadecapole configuration [s,p^-,$^\circ_|$] on the extreme left to the polar, spherical-projectile oblate-target configuration [s,o,$^\circ_|$] on the far right.

In Fig. 2 we show the five different limiting orientations that occur for fixed target and projectile deformation for the case where both target and projectile have prolate

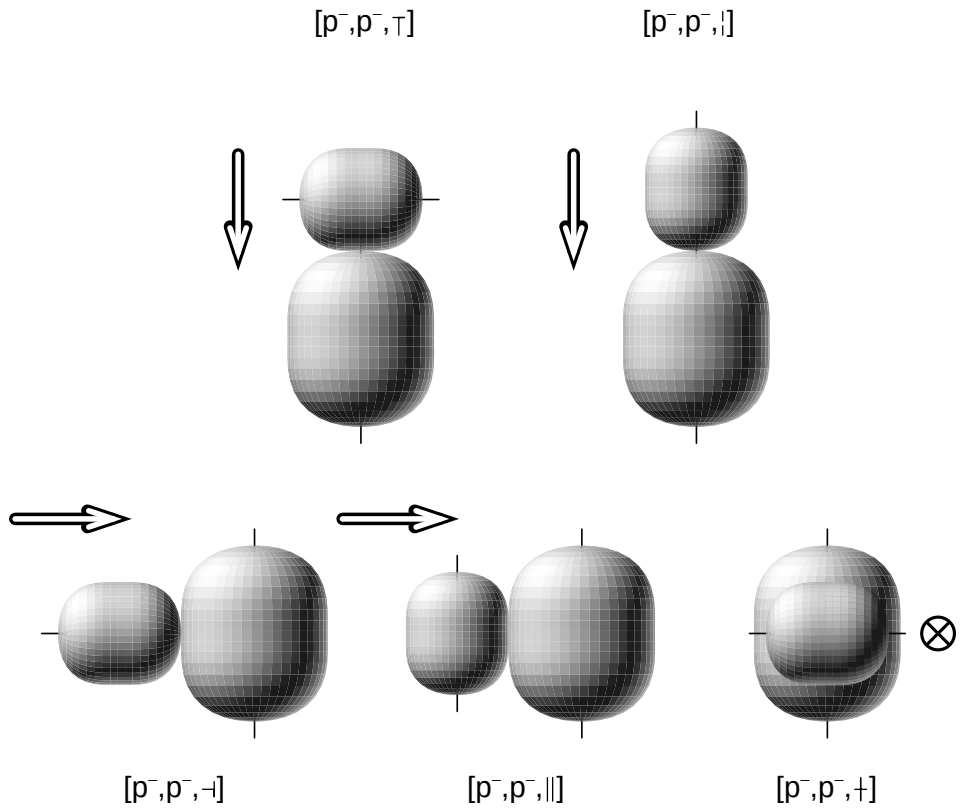

Figure 2. Five limiting touching configurations with prolate, negative-hexadecapole projectiles and targets. Specifically $\beta_2 = 0.24$ and $\beta_4 = -0.09$. The ratio between the projectile and target volume is 0.343. Only the relative positions and orientations change between the configurations. The arrows give the direction of the incident beam. The nuclear symmetry axis is indicated by a thin line emerging from the nuclear polar regions.

deformation with large negative hexadecapole momnents. In our classification scheme 45 different configurations occur when both the projectile and target are deformed and of unequal mass. In the case of equal projectile and target mass the configuration [p^+,p^-,⊤] and [p^-,p^+,⊣], for example, are identical. Indeed, in this case all the configurations [p^-,p^+,any] have a corresponding configuration [p^+,p^-,any], and other similar correspondences also occur. Therefore, for equal-mass projectile-target combinations the configurations [p^+,p^+,⊤], [p^-,p^-,⊤] and [o,o,⊤] are equivalent to [p^+,p^+,⊣], [p^-,p^-,⊣] and [o,o,⊣], respectively. This is the reason there are only 27 different configurations when the projectile and target are of equal mass.

In Figs. 1 and 2 we use the β parameterization to describe the nuclear shape. Volume conservation has not been applied in these and subsequent figures of nuclear shapes, but this is an insignificant approximation since volume conservation only changes R_0 by fractions of a percent for the deformations considered. However, in energy calculations it is essential to include volume conservation, as we do in our calculations here. As representative defor-

mations we make the following choices. As the prolate–positive hexadecapole deformation p^+ we choose $\beta_2 = 0.30$ and $\beta_4 = 0.11$. This corresponds to the experimentally determined deformation of ^{154}Sm [12]. The prolate-negative hexadecapole deformation p^- is chosen as $\beta_2 = 0.24$ and $\beta_4 = -0.09$, corresponding to the experimentally determined deformation of ^{186}W [12]. Finally, as a representative oblate deformation we have selected $\beta_2 = -0.25$ and $\beta_4 = 0.0$. The ratio between R_0 of the projectile and target is 0.7.

3. Deformation and heavy-ion collisions

Although the implications of deformation on cross sections for superheavy-element production have not been very extensively considered so far, deformation certainly is already known to affect fusion cross sections leading to somewhat lighter compound systems. For example, a clear signature of the importance of deformation effects in heavy-ion reactions is the enhancement of sub-barrier fusion cross sections, for which deformation often plays a major role. It may be useful to observe that the designation sub-barrier is somewhat of a misnomer. An implicit assumption behind this designation is that both projectile and target nuclei are spherical. Furthermore, if the measured cross section at energies below the maximum of this assumed spherical fusion barrier is higher than the calculated cross section for this configuration then the term *enhanced sub-barrier fusion* is used. In a more realistic picture one can in many cases show that (1) the energy is not sub-barrier and (2) the measured cross section is not enhanced. To illustrate these features we select the reaction ^{16}O + ^{154}Sm.

3.1. Deformation and the fusion potential-energy surface

We present in Table 1 four fusion-barrier quantities for particular orientations between the projectile and target. Each line corresponds to one orientation and one incident direction. The first eight columns specify the projectile and target nuclei and the deformation used for these nuclei in the calculation of the fusion barrier. The shapes of the projectile and target are given in the Nilsson perturbed-spheroid parameterization [11]. The next column gives the relative orientation of projectile and target in the notation introduced above. The last four columns indicate (1) the distance between the centers of the projectile and target at the maximum of the barrier, (2) the maximum of the fusion barrier, (3) the center-of-mass distance when the projectile and target just touch and (4) the fusion-barrier height at this point.

The first three lines of Table 1 show fusion-barrier data for the reaction ^{16}O + ^{154}Sm. In the first line of the table we show, for reference, the calculated barrier parameters for a hypothetical spherical target shape. The second line gives the fusion-barrier parameters for the configuration [s,p^+,q] corresponding to the equatorial plane $z = 0$ and the third line corresponds to the potential in the [s,p^+,$^\circ_|$] configuration.

3.2. Deformation and fusion cross sections

In Fig. 3 the measured and calculated cross sections corresponding to the reaction ^{16}O+^{154}Sm are presented. The deformed fusion potential is obtained in a model calculation

Table 1. Comparison of entrance-channel fusion configurations. When the sign < is given in the column for $R_{\max}$ and > is given in the column for $V_{\max}$ it means that the maximum of the fusion barrier occurs inside the touching point and consequently is higher than the potential of the touching configuration.

Target				Projectile					Barrier			
	ϵ_2	ϵ_4	ϵ_6		ϵ_2	ϵ_4	ϵ_6	Or.	$R_{\max}$ (fm)	$V_{\max}$ (MeV)	$R_{\rm t}$ (fm)	$V_{\rm t}$ (MeV)
^{154}Sm	0.000	0.000	0.000	^{16}O	0.000	0.000	0.000	○◯	10.54	62.21	9.14	56.22
^{154}Sm	0.250	−0.067	0.030	^{16}O	0.000	0.000	0.000	○|	10.10	63.29	8.80	57.90
^{154}Sm	0.250	−0.067	0.030	^{16}O	0.000	0.000	0.000	° |	11.87	57.18	10.67	53.34
^{150}Nd	0.000	0.000	0.000	^{150}Nd	0.000	0.000	0.000	○◯	<	>	12.33	379.10
^{150}Nd	0.225	−0.067	0.025	^{150}Nd	0.225	−0.067	0.025	┼	<	>	11.74	390.96
^{150}Nd	0.225	0.200	−0.100	^{150}Nd	0.225	0.200	−0.100	┼	11.69	399.51	10.29	383.98
^{150}Nd	0.225	0.100	−0.044	^{150}Nd	0.225	0.100	−0.044	┼	11.66	396.73	10.86	392.38
^{186}W	0.208	0.100	−0.044	^{110}Pd	0.200	0.027	−0.013	⊤	<	>	12.29	358.13
^{186}W	0.208	0.100	−0.044	^{110}Pd	0.200	0.027	−0.013	| |	<	>	13.46	342.61
^{186}W	0.208	0.100	−0.044	^{110}Pd	0.200	0.027	−0.013	⊣	<	>	12.15	359.01
^{186}W	0.208	0.100	−0.044	^{110}Pd	0.200	0.027	−0.013	||	11.69	375.12	10.99	372.84
^{186}W	0.208	0.100	−0.044	^{110}Pd	0.200	0.027	−0.013	┼	11.69	376.20	10.99	374.14
^{186}W	0.000	0.000	0.000	^{110}Pd	0.000	0.000	0.000	○◯	<	>	12.18	361.10
^{192}Os	0.142	0.073	−0.032	^{104}Ru	0.233	−0.013	0.012	┼	11.72	367.82	11.22	367.11

with no free parameters and is the sum of the nuclear and Coulomb potentials according to Ref. [12] and a centrifugal barrier term, which is treated in the spherical limit. The calculated cross section is from a study [13] of fusion cross sections in reactions of spherical projectiles and deformed targets. It has no free parameters except a simple translation in energy of the calculated cross-section curves. The cross section is obtained by integrating over angle the transmission coefficients which are obtained by calculating the barrier penetrability at each angular momentum by use of the WKB approximation. The deformation parameters of the target are obtained from a mass calculation [14]. Obviously there are large deformation effects both in the potential energy and in the fusion cross section. Clearly our model, incorporating significant aspects of deformation, accounts well for the "enhancement" of the cross section relative to the fusion cross section obtained for a hypothetical spherical target, at least for energies down to the Coulomb barrier in the polar direction.

3.3. Gentle fusion?

Because the evaporation residue cross sections in cold fusion between spherical projectiles and targets drop so strongly towards heavier nuclei, Nörenberg [15,16] suggested that "gentle fusion" of two well-deformed rare-earth nuclei in an equatorial-cross orientation ┼ should

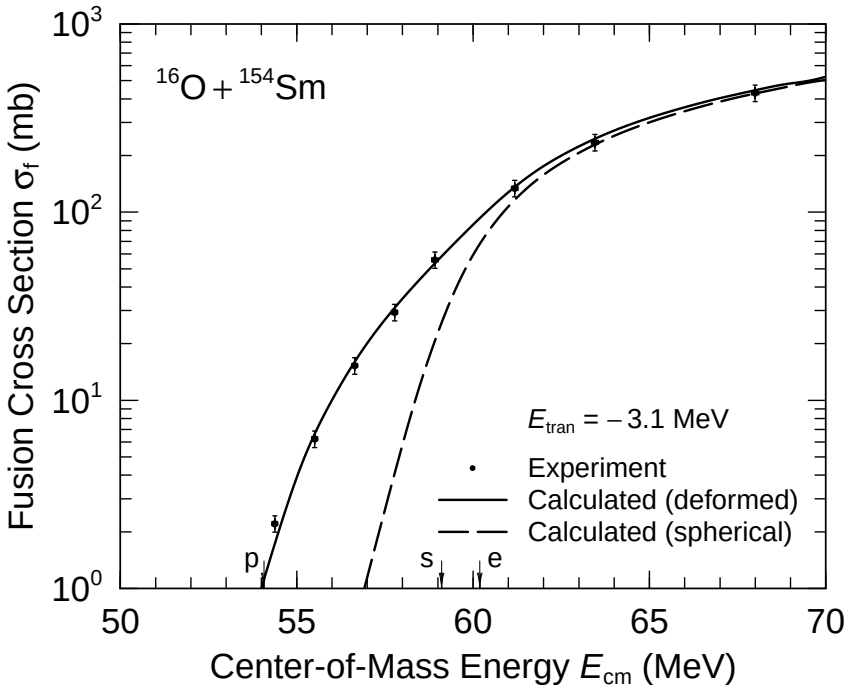

Figure 3. Calculated fusion cross sections for the reaction ^{16}O+^{154}Sm, compared to experimental data. The solid curve corresponds to the calculated fusion cross section obtained when the shape of the target corresponds to the calculated ground-state shape. The long-dashed curve is the cross section obtained for a hypothetical spherical target. The arrows show the fusion-barrier height in the polar direction (p), the equatorial plane (e), and the barrier height for a hypothetical spherical target (s). Both the curves and the arrows have been translated in energy by $E_{\rm tran} = -3.1$ MeV from their calculated values.

be investigated because, he stated, "this orientation leads to the most compact touching configuration out of all possible orientations of the two deformed nuclei." Consequently, the evaporation-residue cross sections may be sufficiently large to allow detection.

We first observe that according to our calculations [14], only the lightest nuclei in the rare-earth region would lead to compound systems with α half-lives over 1 μs, which is the approximate transit time from the target to detection area in the SHIP experimental setup. Already the reaction ^{160}Gd + ^{160}Gd$\rightarrow$ $^{320-xn}$128 + xn leads to nuclei where the calculated [14,17] α-decay half-lives are less than about 0.01 μs. To study the concept of gentle fusion we must therefore select a reaction in the beginning of the rare-earth region, so we choose the reaction ^{150}Nd + ^{150}Nd to illustrate Nörenberg's suggestion. We show the configuration of two ^{150}Nd nuclei with calculated ground-state shapes in Fig. 4. The configuration is [p$^+$,p$^+$, $+$] and is the one proposed by Nörenberg as favorable for SHE production. Calculated fusion-barrier data for the hypothetical spherical case and the configuration in Fig. 4 are found in Table 1, on lines 4 and 5, respectively.

It is clear that the fusion configuration $+$ suggested by Nörenberg is limited to [p$^+$,p$^+$, $+$] configurations, since projectiles and targets must be chosen from the beginning of the rare-earth region. This configuration is not particularly compact relative to a collision

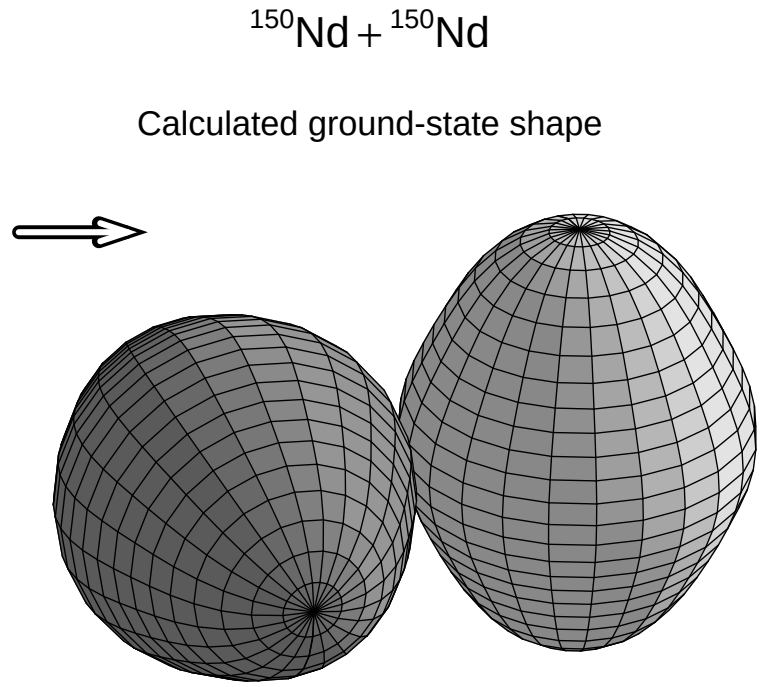

Figure 4. Touching configuration of ^{150}Nd + ^{150}Nd with the nuclear shapes taken to be the calculated [14] ground-state shape; that is, the configuration is [p$^+$, p$^+$,+]. The arrow gives the direction of the incident beam. Fusion-barrier parameters for this configuration/direction are given on line 5 of Table 1.

between similar-size spherical nuclei, as is clear from Fig. 4 and Table 1. Indeed, because of the large negative ϵ_4 of the ground state, which results in a bulging equatorial region and a large positive hexadecapole moment, the configuration in Fig. 4 is quite similar to the spherical configuration. This observation is supported by the quantitative results in Table 1: the distance between mass centers of the gentle fusion configuration is 11.74 fm, only 0.59 fm more compact than the spherical configuration.

The idea that configurations where deformed nuclei touch each other in the equatorial regions are more compact than some other configurations and may therefore be favorable for SHE production is not new. It was for instance mentioned in Ref. [12] in a discussion of the reaction ^{48}Ca + ^{248}Cm, and we will return to this reaction below. Clearly, the fusion barrier for deformed systems along a one-dimensional path will be very different in the polar direction and in an equatorial direction. When the projectile is deformed the fusion barrier will also depend strongly on the orientation of the incident deformed projectile.

It is obvious that when colliding heavy ions have well-developed prolate deformation, then the most compact configurations occur when the point of touching is in the equatorial region of both nuclei. Which relative orientation of the two nuclei, + or ||, is the most favorable is perhaps not known at present. However, the orientation suggested by Nörenberg is one possible favorable configuration, but its properties will depend strongly on the value of the hexadecapole deformation, that is, in our case on the value of the deformation parameter ϵ_4. Large negative values of ϵ_4 correspond to bulging equatorial regions, whereas positive

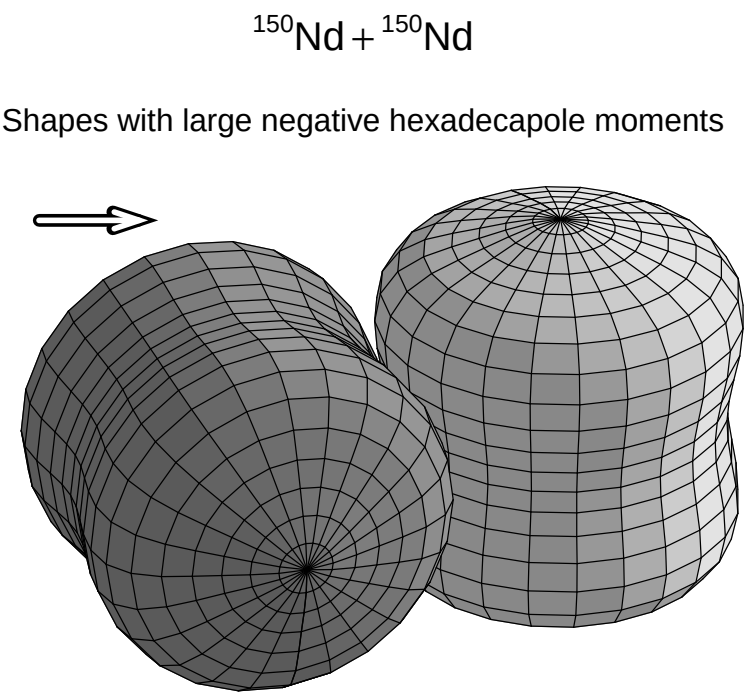

Figure 5. Touching configuration of ^{150}Nd + ^{150}Nd for hypothetical nuclear shapes with a large positive ϵ_4 and a choice of ϵ_6 that further develops the waistline; that is, the configuration is [p$^-$, p$^-$,+]. The arrow gives the direction of the incident beam. Fusion-barrier parameters for this configuration/direction are given on line 6 of Table 1.

values lead to neck formation. We now look at the latter, more compact configurations.

3.4. Hugging fusion!

To clearly illustrate the effect of large positive values of the deformation parameter ϵ_4 we first study an example where we for clarity exaggerate somewhat the effect. We show in Fig. 5 the configuration in Fig. 4, with one change, namely we select ϵ_4 and ϵ_6 so that a well-developed neck results. The configuration is [p$^-$,p$^-$,+]. The corresponding calculated fusion-barrier parameters are listed on line 6 of Table 1. This hypothetical shape is presented to show the effect of a well-developed neck on the fusion barrier and touching configuration. Clearly this configuration is very different from both the spherical configuration and the gentle configuration and quite compact. Similar configurations with necks in the equatorial regions instead of bulging midsections could favor a large cross section for complete fusion. Because the nuclei "grab" each other we call this configuration corresponding to this specific orientation and where both projectile and target exhibit some neck formation *hugging fusion*. In our classification scheme hugging fusion corresponds to the [p$^-$,p$^-$,+] class of touching fusion configurations. The ϵ_4 deformation value selected to clearly show this principle is probably unrealistically large. However, large positive ϵ_4 deformations occur in the end of the rare-earth region. To compare the effect of a realistic positive value of ϵ_4 with the effect of a large negative ϵ_4 we apply the deformation calculated [14] for ^{186}W to ^{150}Nd

and obtain the fusion barrier given on line 7 of Table 1. We see that the distance between mass centers of this configuration is only 10.86 fm, that is, 1.47 fm more compact than the spherical configuration and 0.88 fm more compact than a configuration with a large negative ϵ_4. To exploit the enhancement of the evaporation-residue cross section that we expect in the hugging configuration [p$^-$,p$^-$,+] we must find suitable projectiles and targets with large positive ϵ_4 ground-state deformations that lead to superheavy elements with half-lives that are sufficiently long that the evaporation residues are observable.

4. Heavy-ion reactions for distant superheavy-element production

The most stable nuclei on the superheavy island are predicted to occur in the vicinity of $^{288-294}110$ even though the magic proton number in this region is calculated to be 114 [17]. However, nuclei at some considerable distance away from the center of the island are calculated to be sufficiently long-lived to allow observation after formation; that is, they are predicted to have half-lives in excess of 1 μs. We refer to elements with proton number larger than 114 as distant superheavy elements. We now look at some heavy-ion reactions that may lead to this far part of the superheavy island.

4.1. Hugging fusion candidates for distant superheavy-element production

Above we noted that to achieve very compact configurations of deformed nuclei one should find projectiles and targets with large positive values of the ϵ_4 deformation parameter. Clearly then, the best candidates for a stable target above proton number 50 would be nuclei near the end of the rare-earth region. To be specific, we select ^{186}W as a target in our first example. For this nucleus, calculations [14] give $\epsilon_4 = 0.100$ and $\epsilon_6 = -0.044$. The large negative value of ϵ_6 also contributes to the development of a neck. A suitable projectile that would take us to the region of distant superheavy elements would then be ^{110}Pd leading to the compound system $^{296}120$. The hugging configuration for this choice is shown from four different angles in Fig. 6. The fusion barrier for the hugging configuration [p$^-$,p$^-$,+] is listed on line 12 of Table 1, where we to illustrate the orientation effect on the fusion barrier also list the barrier parameters for the four other deformed configurations [p$^-$,p$^-$,⊤], [p$^-$,p$^-$,|], [p$^-$,p$^-$,⊣] and [p$^-$,p$^-$,||] on lines 8–11. These five deformed configurations also appear in Fig. 2 for slightly different projectile-target sizes and deformations. The table listing on lines 8–12 is in the order the configurations occur in Fig. 2. In Table 1 we also list on line 13, for reference, the barrier parameters for the [s,s,∝◯] configuration.

To make an estimate of the decay properties of the compound system we make the following assumptions. The heavy-ion reaction takes place at the fusion-barrier energy. We do not calculate the branching ratio between fusion-fission and complete fusion, but are primarily interested in studying the alpha-decay rates of the compound nuclei that possibly do not fission but de-excite by neutron emission. One expects of course that at high excitation energy some washing out of shell effects has taken place and that Γ_f/Γ_n is large. It is a remaining, important problem to calculate this quantity. We assume that neutrons are emitted as long as energetically possible. The Q-values and masses required for these calculations are obtained from Ref. [14]. The α-decay half-lives are calculated as discussed in Ref. [17]. With these assumptions we find for the reaction and configuration

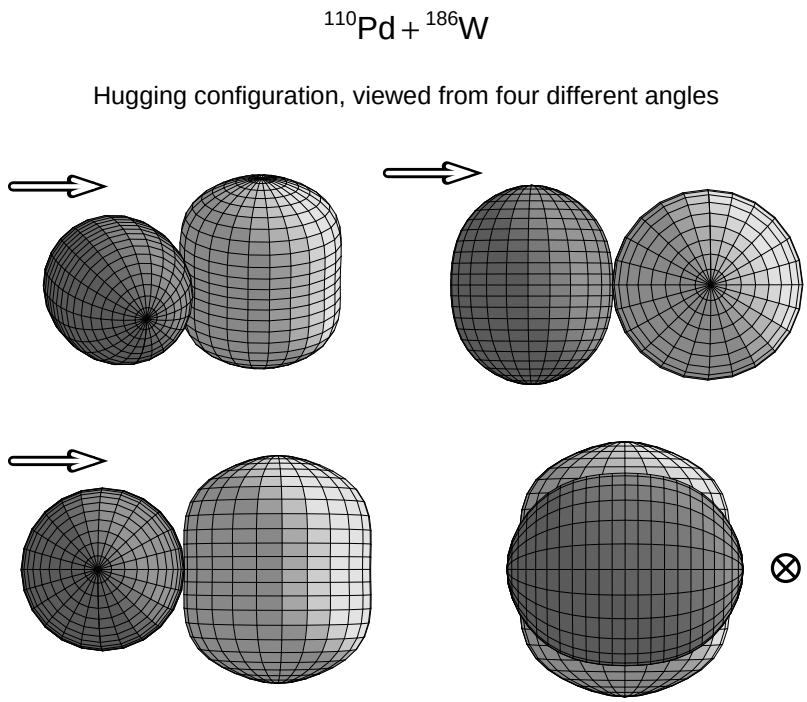

Figure 6. Touching configuration of ^{110}Pd + ^{186}W for calculated ground-state shapes viewed from four different angles. The shapes used are the calculated ground-states shapes, so the configuration is [p$^-$,p$^-$,+]. The arrows and $\otimes$ sign give the direction of the incident beam. Fusion-barrier parameters for this configuration/direction are given on line 12 of Table 1.

[p$^-$,p$^-$,+] shown in Fig. 6 at a center-of-mass energy equal to the Coulomb barrier energy listed on line 12 in Table 1 that two neutrons are emitted. Thus

$$^{110}\mathrm{Pd} + {}^{186}\mathrm{W} \rightarrow {}^{296}120^* \rightarrow {}^{294}120 + 2\mathrm{n} \qquad (2)$$

where the compound nucleus has an excitation energy of 35.04 MeV before neutron emission. The α-decay-chain half-lives and Q-values are shown in Fig. 7. Although the first few decays are calculated to be only a few μs, these decays should be within the detection limit of SHIP. Fission half-life calculations are characterized by large uncertainties [17], but the calculated ground-state microscopic corrections in the region of the compound system are about -7 MeV, so one expects a fission barrier about this high in this region of nuclei. Such a high barrier would probably be associated with fission half-lives that are longer than the calculated α half-lives down to about element 104 for all the decay chains considered here.

We have also considered the reaction

$$^{104}\mathrm{Ru} + {}^{192}\mathrm{Os} \rightarrow {}^{296}120^* \rightarrow {}^{294}120 + 2\mathrm{n} \qquad (3)$$

The barrier parameters are listed on line 14 in Table 1. A beam energy equal to the Coulomb barrier value of 367.82 MeV leads to a compound-nucleus excitation energy of 34.06 MeV, which is about 1 MeV lower than in the reaction (2), and consequently to the same α-decay sequence after 2n emission.

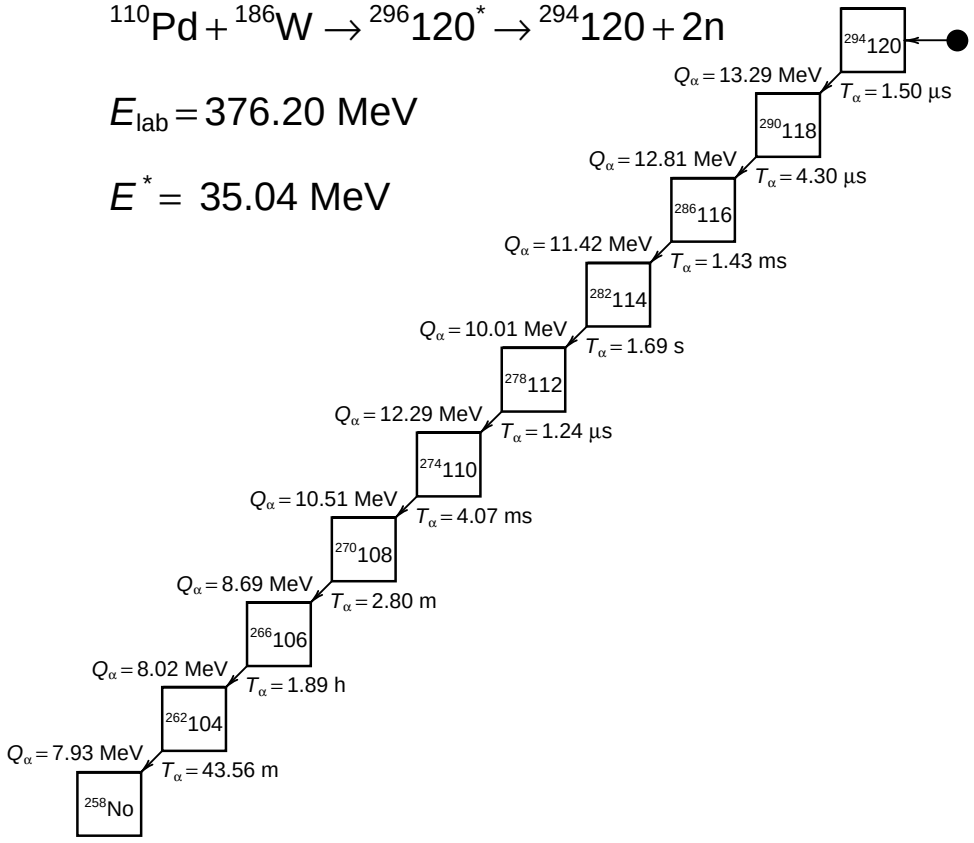

Figure 7. Calculated Q-values for α decay and corresponding calculated half-lives for the decay chain starting at $^{294}120$.

5. Summary

In heavy-ion collisions between deformed projectiles and targets we have shown that the fusion reaction depends strongly on the relative orientation of the projectile and target. Both the fusion-barrier height and the compactness of the touching configuration are so strongly affected that a variation of relative orientation may have a similar impact as varying the projectile and/or target nuclear species. Therefore, a detailed consideration of deformation is necessary in both theory and experimental work so that we can understand more about the many features of heavy-ion reactions between deformed nuclei. To facilitate such studies we have introduced a classification scheme of deformed fusion configurations.

Systematic experimental work on understanding cold-fusion reactions and associated cross sections for evaporation-residue formation and parallel investigations of microscopic nuclear-structure models have over the last 20 years or so led to the discovery of five new elements on the side of the superheavy island closest to us. Similar or more extensive work will be required to describe in detail the fusion reactions between two deformed nuclei. However, the reward may be access to the far side of the superheavy island. Of particular

interest is to study how the high charge numbers of these nuclei affect nuclear and atomic properties. Above we have given a few examples of heavy-ion reactions that could serve as particularly suitable starting points for exploring both theoretically and experimentally the new physics of deformed heavy-ion reactions, and possibly the new physics of the far side of the superheavy island. In particular we have suggested that a few special fusion configurations may be especially favorable for forming superheavy elements. In hot fusion, we suggest as most favorable an asymmetric projectile-target combination in the *hugging* configuration [$p^-, p^-, +$].

A more extensive discussion of the ideas presented here may be found in Ref. [18].

This work was supported by the Japan Atomic Energy Research Institute and by the U. S. Department of Energy.

References

[1] G. Münzenberg, S. Hofmann, F. P. Heßberger, W. Reisdorf, K.-H. Schmidt, J. R. H. Schneider, P. Armbruster, C.-C. Sahm, and B. Thuma, Z. Phys. **A300** (1981) 7.

[2] G. Münzenberg, P. Armbruster, H. Folger, F. P. Heßberger, S. Hofmann, J. Keller, K. Poppensieker, W. Reisdorf, K.-H. Schmidt, H. J. Schött, M. E. Leino, and R. Hingmann, Z. Phys. **A317** (1984) 235.

[3] G. Münzenberg, P. Armbruster, F. P. Heßberger, S. Hofmann, K. Poppensieker, W. Reisdorf, J. R. H. Schneider, W. F. W. Schneider, K.-H. Schmidt, C.-C. Sahm, and D. Vermeulen, Z. Phys. **A309** (1982) 89.

[4] S. Hofmann, N. Ninov, F. P. Heßberger, P. Armbruster, H. Folger, G. Münzenberg, H. J. Schött, A. G. Popeko, A. V. Yeremin, A. N. Andreyev, S. Saro, R. Janik, and M. Leino, Z. Phys. **A350** (1995) 277.

[5] S. Hofmann, N. Ninov, F. P. Heßberger, P. Armbruster, H. Folger, G. Münzenberg, H. J. Schött, A. G. Popeko, A. V. Yeremin, A. N. Andreyev, S. Saro, R. Janik, and M. Leino, Z. Phys. **A350** (1995) 281.

[6] J. R. Nix and A. J. Sierk, Phys. Scr. **10A** (1974) 94.

[7] J. R. Nix and A. J. Sierk, Phys. Rev. **C15** (1977) 2072.

[8] J. Błocki, Y. Boneh, J. R. Nix, J. Randrup, M. Robel, A. J. Sierk, and W. J. Swiatecki, Ann. Phys. (N. Y.) **113** (1978) 330.

[9] K. T. R. Davies, A. J. Sierk, and J. R. Nix, Phys. Rev. **C28** (1983) 679.

[10] P. Möller and J. R. Nix, Nucl. Phys. **A272** (1976) 502.

[11] S. G. Nilsson, Kgl. Danske Videnskab. Selskab. Mat.-Fys. Medd. **29**:No. 16 (1955).

[12] P. Möller and A. Iwamoto, Nucl. Phys. **A575** (1994) 381.

[13] A. Iwamoto and P. Möller, to be published (1995).

[14] P. Möller, J. R. Nix, W. D. Myers, and W. J. Swiatecki, Atomic Data Nucl. Data Tables **59** (1995) 185.

[15] W. Nörenberg, Proc. Int. Workshop on Heavy-Ion Fusion, Padua (1994).

[16] W. Nörenberg, GSI Nachrichten 10-94 (Oct. 1994) p. 13.

[17] P. Möller and J. R. Nix, J. Phys. G: Nucl. Part. Phys. **20** (1994) 1681.

[18] A. Iwamoto, P. Möller, J. R. Nix, and H. Sagawa, Nucl. Phys. **A**, to be published.